Near-surface effects at the antiferromagnetic phase transition in uranium phosphide

A. Stunault
European Synchrotron Radiation Facility, Boîte Postale 220, F38043 Grenoble, France

S. Langridge
European Synchrotron Radiation Facility, Boîte Postale 220, F38043 Grenoble, France and Commission of the European Communities, Joint Research Centre, Institute for Transuranium Elements, D-76125 Karlsruhe, Germany

C. Vettier
European Synchrotron Radiation Facility, Boîte Postale 220, F38043 Grenoble, France

D. Gibbs
Department of Physics, Brookhaven National Laboratory, Upton, New York 11973

N. Bernhoeft
European Synchrotron Radiation Facility, Boîte Postale 220, F38043 Grenoble, France
(Received 6 March 1996; revised manuscript received 21 March 1996)

A careful investigation of the resonant x-ray magnetic-scattering response in uranium monophosphide reveals the crucial role played by magnetization density correlations in the discontinuous paramagnetic to antiferromagnetic phase transition in this material. The magnetization density correlations, which are measured on the short time scale typical of the resonant x-ray-scattering technique, appear highly anisotropic in their inferred spatial distribution. Such correlated regions exist in the near-surface regime probed by the low-energy x-ray beam (3.278 keV) and exhibit strongly temperature-dependent behavior at and above the bulk phase transition. For specular reflections this leads to well defined two length scale diffraction profiles in the vicinity of the phase transition and, when taken with the off-specular data, to a phenomenological model which suggests that the extended length scale of near-surface antiferromagnetism may arise from a localized surface distortion. This type of model may be more generally useful both in the two length scale problem and in other systems where defects or fluctuations may, in a similar manner, drive pseudo-long-range order.
[S0163-1829(97)08401-4]

I. INTRODUCTION

A. Motivation for the study

Unusual and strongly temperature-dependent diffraction profiles observed in the vicinity of structural and magnetic phase transitions continue to arouse interest.[1–5] Pioneering studies by neutron-diffraction,[6] x-ray diffraction,[7–10] and theoretical methods[11] revealed the possibility of non-Lorentzian line shapes in the immediate vicinity of the phase transition and acted as a stimulus to a host of recent studies on magnetic systems. These experimental studies have become possible through the combined discovery of resonant magnetic x-ray diffraction and the availability of synchrotron-radiation light sources. In turn the data have activated much theoretical interest. In the following we report on the contribution that resonant magnetic x-ray-diffraction studies of the *discontinuous* paramagnetic to antiferromagnetic phase transition in the uranium monopnictides may make to this problem.

The monopnictides of interest have a simple NaCl crystal structure and transform in an apparently discontinuous manner from the disordered paramagnetic state to a simple (commensurate) type-I antiferromagnetic state with a propagation vector along equivalent $\langle 001 \rangle$-type directions and moments parallel to the propagation vector. That is, the antiferromagnetic state consists of alternate up and down sheets of ferromagnetically aligned moments, wherein the moment direction is perpendicular to the sheet and parallel to one of the original cubic axes. Although the phase transition must be accompanied by a tetragonal distortion, in practice it is so weak that we continue to use cubic indexing in discussion. On account of the symmetry such layers are expected to occur in three equally populated domains along the three, orthogonal, cubic axes in the antiferromagnetic state of an infinite crystal. Any one domain is thus an approximate realization of the antiferromagnetic metamagnetic state or of ''super-antiferromagnetism''[12,13] on which much theoretical attention has been placed, especially with regard to the nature of the phase transition, possible tricritical points under the application of an external field, and the high-temperature series expansions of the bulk susceptibility.[14,15]

B. Previous work on uranium phosphide (UP)

Of the systems which may be taken as physical realizations of the super-antiferromagnetic phase, we have studied a series of single crystals of high crystalline perfection of composition UAs and UP. Preliminary results for the line shapes

of resonantly magnetically diffracted x-ray beams from UAs have been reported;[16] in this communication we focus on the compound UP. While the monopnictide and arsenide readily form crystals to sizes of the order of millimeters the monophosphide is much more reluctant to grow and is consequently less studied. Nevertheless, previous work on UP includes neutron diffraction, NMR, magnetization, resistivity, heat-capacity studies, and volumetric measurements.[17] Both through bulk properties such as the magnetic susceptibility and through microscopic measurement of the staggered magnetization (order parameter) by magnetic neutron scattering, a discontinuous transition from paramagnetic to antiferromagnetic order has been established at a temperature close to $T_n \sim 120$ K. In common with data collected on the neighboring arsenide and pnictide these probes give evidence for anomalous dynamical behavior of the magnetization density in both the antiferromagnetically ordered and paramagnetic phases of UP. Such effects are already apparent in the electrical resistivity, which increases slightly with decreasing temperature in the paramagnetic state,[18,19] and the NMR investigations which yield evidence for a large energy scale of magnetic fluctuations which may be characteristic of strongly coupled $5f$ and conduction-electron states.[20,21] These findings are substantiated in the ordered state by an anomalously large linear term in the electronic specific-heat coefficient $\gamma = 32$ mJ mol^{-1}K^{-2},[22] the strongly reduced low-temperature moment of 1.74 μ_B/uranium ion in comparison with a Curie-Weiss-like effective moment of 3.3–3.4μ_B,[23–26] and the results of recent low-temperature NMR studies.[27] However, as in the arsenide, despite careful searches no studies to date give direct measure of the tetragonal distortion upon entering the antiferromagnetic phase from the paramagnetic state.[28,29] In summary, from the available literature one is led to conclude that UP undergoes a transition of a discontinuous nature from the paramagnetic to a simple type-I antiferromagnetic state without a severe lattice distortion and that there exist important electronic correlations which may play upon the magnitude of the sublattice magnetization density both below and above T_n.

C. Scope of present measurements

It has been suggested that ''second length scale,'' that is to say anomalously sharp, diffraction profiles in the vicinity of a magnetic phase transition reflect the presence of near-surface-induced (antiferro) magnetism.[1–5] The sensitivity of such a state to sample surface preparation has been demonstrated[2] as has the location of the effect to a near-surface regime with a range variously estimated to extend from some hundreds of Ångstroms[2] to some hundred micrometers[4,30] below the nominal sample surface. On approaching a continuous phase transition the presence of such a near-surface (antiferro) magnetic layer taken in conjunction with the diverging correlation length will tend to polarize the underlying material with the result that the bulk magnetic response is merged into that of the surface layers making the separation of the two effects difficult. A cleaner study of near-surface magnetism may be possible in materials with relatively short and temperature-independent thermodynamic correlation lengths such as may exist at a transition of a discontinuous nature. Using a near-surface sensitive probe to investigate a discontinuous phase transition one would hope to distinguish the following regimes: a near-surface magnetic layer above a paramagnetic bulk (the short length scale thermodynamic correlations should give a relatively weak and temperature-independent signal in this interval), a region of coexistence of surface and bulk (ordered) magnetism where one may hope to observe a two-component diffraction profile and finally, at low temperatures, a diffraction profile dominated by the ordered bulk. In view of this we have examined in some detail the contribution that resonant magnetic x-ray-diffraction data of the discontinuous paramagnetic to antiferromagnetic phase transition in the uranium monopnictides may make to our understanding of the antiferromagnetic phase transition and the observation of two length scale diffraction profiles.

The technique of resonant magnetic x-ray diffraction has been developed extensively over the past ten years and has proven exceptionally useful in the investigation of large length scale fluctuations of antiferromagnetic correlations in the rare-earth and actinide compounds.[31–33] The sensitivity arises from the resonant enhancement of the x-ray scattering cross section which occurs on tuning the incident x-ray energy near the L and M absorption edges of the heavy-metal components coupled with transition selection rules which reflect the magnetic state of the heavy-metal ion.[34–36] For uranium compounds large enhancements are found to occur at the M edges. In particular, previous studies at the M_{IV} edge of uranium in the related compound UAs have shown the dominant scattering to be electric dipolar in nature and to lead to measured magnetic intensities as large as 1% of the typical charge peaks.[31–33]

Our x-ray resonant scattering investigations of the magnetic-diffraction profiles supplement the previous findings in UP and strongly suggest the important role that near-surface-induced magnetism may play in the formation of the antiferromagnetic state. The idea for these experiments was prompted by preliminary results obtained on UAs (Ref. 16) and the consideration of the role played by the discontinuous phase transition as outlined above. The rest of the paper is organized as follows: Sec. II gives physical details of the sample and the diffractometer used in this study in addition to presenting the key experimental result of the paper, the observation of an anisotropic two length scale diffraction profile occurring in the immediate vicinity of the antiferromagnetic phase transition. The neutron-scattering data alluded to both in this section and elsewhere in this paper has been instrumental in generating the point of view adopted, however, it represents a sufficiently different and detailed study that we feel obliged to present it fully in a separate publication.[37] Section III offers an interpretation of the resonant two length scale line shape based on as complete as possible analysis of the available x-ray data. In particular, we address the anisotropic nature of the scattering profile in the longitudinal and transverse directions within the scattering plane and attempt an analysis including the thermal evolution of the magnitude of the effective sublattice magnetic scattering moment. In Sec. IV a summary of the interpretation of the data is given together with an analysis of a simple Ginzburg-Landau model which illustrates the possibility of generating near-surface (antiferro)-magnetism above a discontinuous phase transition. This type of model may be ex-

tended to other systems where defects or fluctuations may, in a similar manner, drive pseudo-long-range order. Finally, Sec. V offers a summary and comparison with other two length scale results by way of a conclusion.

II. EXPERIMENTAL TECHNIQUE AND SUMMARY OF DATA

A. Sample preparation and characterization

Despite the difficulty in obtaining single-crystal samples, UP was chosen for this study since, unlike UAs, it gives no evidence, neither in its bulk properties nor in magnetic-diffraction data for an incommensurate precursor magnetic phase above T_n.[38] This makes possible an analysis of the diffraction profiles with a minimum of parameters which in turn motivates a simple qualitative model of the phase transition (Sec. IV). The sample is that characterized in the previous neutron-diffraction studies of Burlet *et al.*[39] Details of sample preparation, given in detail by Horyn, Henry, and Rossat-Mignot,[40] are briefly as follows. An initial reaction at 800–850 °C to form UP_2 was followed by decomposition at 1700 °C to yield the UP precursor. This route was developed on account of the high chemical reactivity of the constituent elements and the high melting point of the compound (in the region of 2500 °C). The resulting UP precursor was dissolved in a gallium flux and slowly cooled in a temperature gradient at 1100 °C over a period of one month to yield a set of small single crystals. X-ray microprobe analysis indicated the resulting crystals to be free of gallium contamination. Although no detailed studies have been carried out, preliminary investigations of crystalline quality on a rotating anode spectrometer and the results presented in this paper, indicate a crystal mosaic of the order of 0.05° full width at half maximum (FWHM).

We further characterized the crystals selected for our experiments by their induced bulk magnetic moment in applied fields ranging between 100 and 2000 G over the temperature interval 4.2–300 K as measured in a superconducting quantum interference device magnetometer of the Quantum design at the CEA Grenoble. The observed bulk magnetic behavior of the UP samples is as follows (see Fig. 1). On heating, UP exhibits a sharp discontinuous increase in induced moment at a temperature of 120 K which is followed by a plateau region extending over some 10 K, smooth fall, and Curie-Weiss-like behavior. The response of UP at high temperatures is thus generically of the form of that observed in antiferromagnetic metamagnets and calculated in, for example, the series expansions of metamagnetic Ising-like models.[12,13] This simple high-temperature behavior, in contrast to that observed in UAs,[38] is consistent with the absence of an incommensurate magnetic precursor phase.

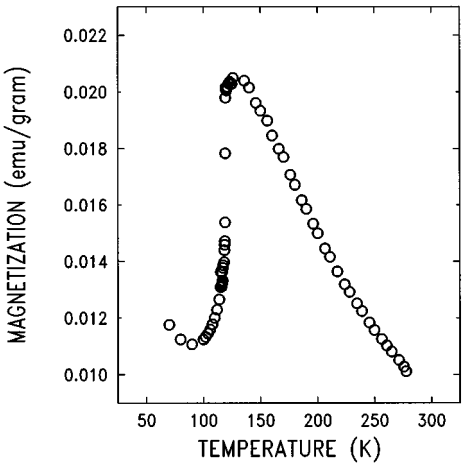

FIG. 1. The induced magnetization in UP under an applied field of 500 G as a function of temperature. The applied field direction is approximately parallel to a fourfold axis. The antiferromagnetic phase transition at 120 K is clearly defined and from the high-temperature behavior one extracts a Curie-Weiss moment of $3.4\mu_B$ per uranium atom. The estimated error in a given data point is approximately represented by the size of the symbol.

B. X-ray measurements and integrated intensities

The resonant x-ray-diffraction measurements were carried out on the X22C beamline of the National Synchrotron Light Source, Brookhaven, which is equipped with a toroidally focusing mirror and a double-crystal Ge(111) monochromator. The sample was cleaved along a {001}-type plane to yield a scattering surface of the order of a few square millimeters shortly before insertion into a displex refrigerator, which in turn was mounted on a four-circle diffractometer scattering in the vertical plane. Care was taken to minimize backgrounds and absorption by avoiding air in the optical pathways; this is necessary on account of the high attenuation of the low-energy photon beam by nitrogen at atmospheric pressure. The incoming polarization of the synchrotron radiation, derived from a bending magnet source, is horizontal and perpendicular to the vertical scattering plane. In this scattering geometry the $[00l]$ and $[h00]$ crystallographic directions lie in the scattering plane, respectively, parallel and perpendicular to the surface normal. To maximize the intensity in the magnetically sensitive signal we tuned the spectrometer to the M_{IV} absorption edge of uranium which we experimentally located at 3.728 keV (Fig. 2). In view of the severe penalties in intensity no discrimination of the outgoing polarization was carried out. However, from the resonant

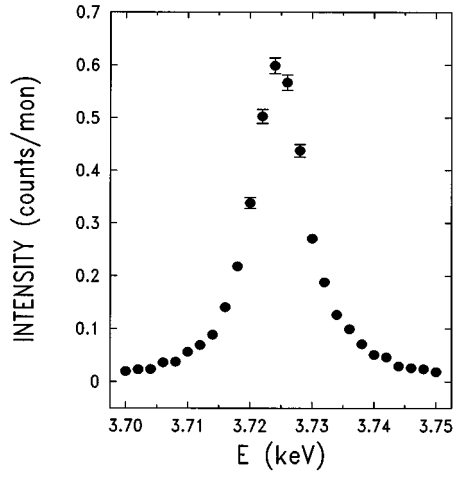

FIG. 2. Incident photon energy scan around the uranium M_{IV} resonance at the antiferromagnetic reflection centered on the (003) Bragg position.

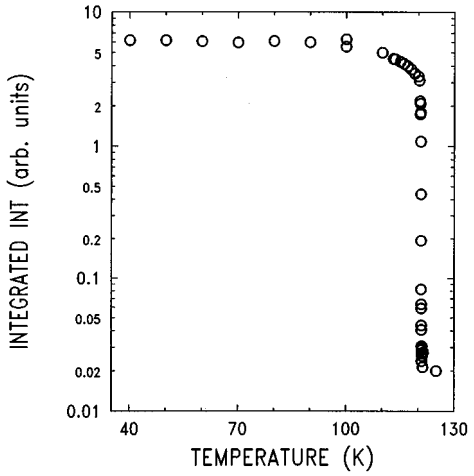

FIG. 3. The integrated intensity in arbitrary units along the specular rod of scattering at the (003) reflection as a function of sample temperature.

nature of the observed signal and previous work[31–33] we are confident that the signal is indeed magnetic in origin. (This conclusion is further corroborated by the overall temperature dependence of the signal shown in Fig. 3 and discussed below.) The combination of a relatively long resonant wavelength coupled with a moderately high lattice parameter (5.588 Å) severely limits the accessible area of reciprocal space for data collection. In particular, in the specular scan direction only the first two antiferromagnetic positions at (001) and (003) can be reached, and the off-specular scans were limited to that at the (102) Bragg position. We restrict our analysis of specular scans to the (003) reflection on account of the superior signal-to-noise ratio attainable compared with (001).

The measured temperature dependence of the integrated resonant intensity along the specular rod around the (003) reflection below the antiferromagnetic to paramagnetic phase transition is shown in Fig. 3 from which we confirm that the signal reflects, in a characteristic manner, the degree of antiferromagnetic order in the sample. Interestingly, no significant high-temperature ''tail'' is seen to develop as has been reported, for example, in UO_2,[2] nor is any hysteresis evident. The integrated intensities for the off-specular (102) reflections which probe magnetic correlations from those domains with a propagation vector lying in the surface plane of the sample are, at a given temperature, significantly weaker than those at the (003) reflection. From our analysis (Sec. III) this difference in intensity arises primarily from the experimental resolution.

C. X-ray magnetic-scattering line shapes

As outlined in the introduction and made evident by the neutron-diffraction studies,[37] the antiferromagnetic phase exhibits domains of moment alignment parallel to the three orthogonal cubic axes. Through the width in reciprocal space of the measured response (down to the resolution limit) we infer the spatial extent of magnetic domains located within the near-surface volume probed by the x-ray beam. The domains have a propagation wave vector either normal to, or in the plane of, the surface. The response localized around the specular antiferromagnetic peak is selectively sensitive to those domains having an ordering wave vector parallel to the surface normal, while in the (102) scattering geometry we probe the response from domains composed of planes of alternating moments with a propagation vector normal to the sample surface. From the relative intensities of scans taken at different temperatures we estimate the effective scattering moment standardized to the low-temperature value in the antiferromagnetic phase.

Data at the resonant energy from UP taken about the (003) antiferromagnetic Bragg point is shown at temperatures below and above the bulk phase transition for both the $[00l]$ and $[h00]$ scan directions in Fig. 4. These data illustrate the key components of behavior observed in UP for the specular reflection. For scans along the specular rod one has a sharp and broad component associated with the low- and high-temperature response, respectively. As we shall see in detail, there exists a well defined region of temperatures in which both the sharp and broad responses coexist and we have a classic two length scale line shape. In the orthogonal

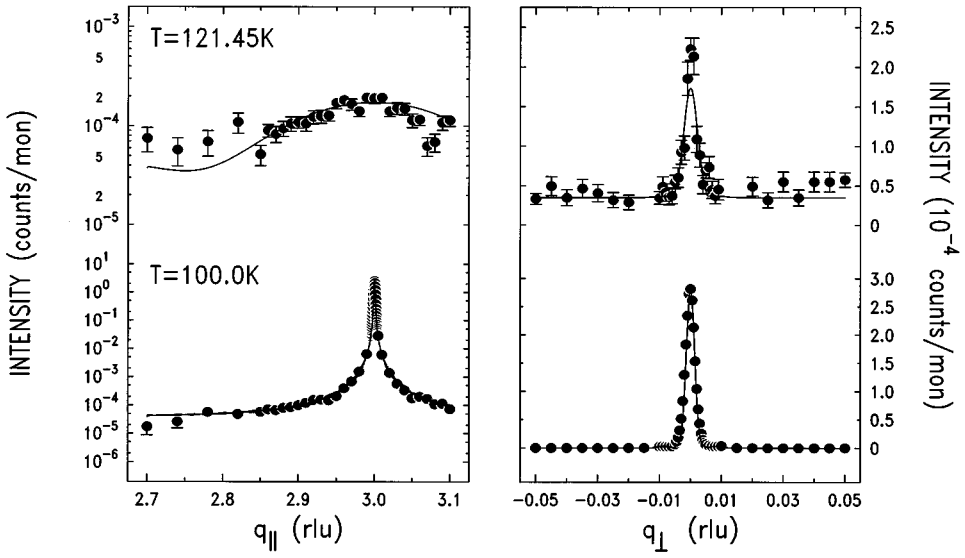

FIG. 4. Longitudinal scans along the specular rod at 100 K well within the antiferromagnetic phase and, at 121.45 K, above the Néel temperature. The dramatic decrease in width on cooling reflects the increasing number of antiferromagnetically correlated layers forming parallel to the sample surface. Scans in the transverse direction through the (003) lattice point have more similar widths indicating that the antiferromagnetic layers forming above the Néel temperature already display a degree of long-range coherence in the surface plane of the sample.

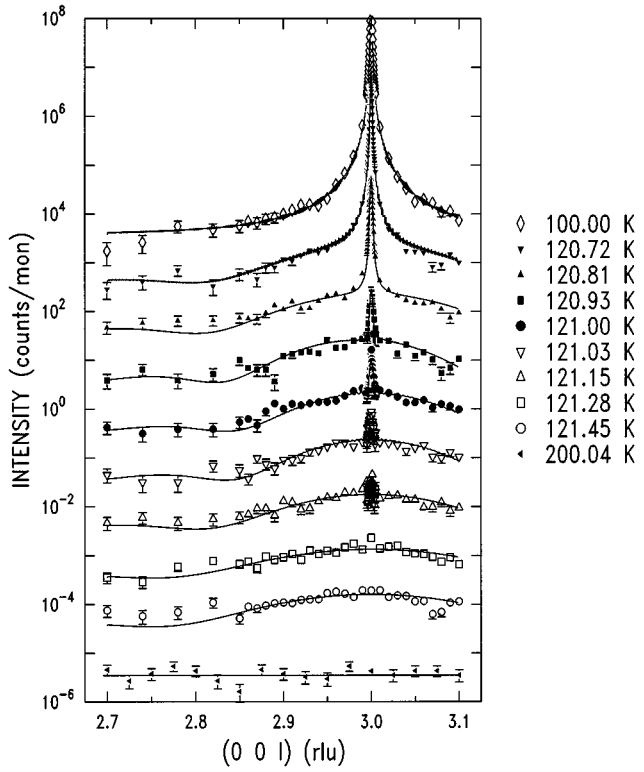

FIG. 5. Temperature dependence of the specular intensity for a selection of scans at the (003) position taken in cooling. The wave-vector transfer is parallel with the ordering wave vector. The vertical axes of consecutive temperatures have been displaced by an order of magnitude to improve visibility. The solid lines are the results of fits to the model function given in Sec. III. An evolution of rounded maxima at elevated temperatures of a broad component into a two-component sharp plus broad line shape around T_n (120.9 K) is seen with the sharp component being typically 100 times narrower than the broad. This two length scale line shape is in turn dominated by the sharp component at low temperatures.

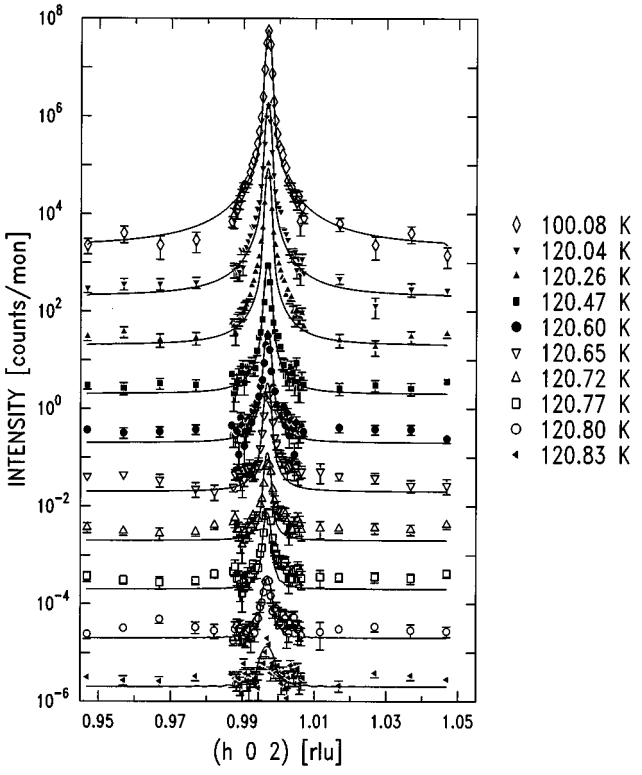

FIG. 6. Temperature dependence of the off-specular intensity for a selection of scans at the (102) position taken in cooling. The wave-vector transfer is parallel with the ordering wave vector. The vertical axes of consecutive temperatures have been displaced by an order of magnitude to improve visibility. The solid lines are the results of fits to the model function given in Sec. III. In contrast with Fig. 5 no broad component is observed.

scans transverse to the specular rod, taken within the vertical scattering plane, the scattering remains essentially sharp over the full range of temperatures studied save for those points in the immediate vicinity of the phase transition.

In Fig. 5, we show the overall temperature dependence of the specular scans in the $[00l]$ direction around the (003) point, on a displaced logarithmic scale, taken in cooling. The continuous lines are fits to the model cross section described in detail in Sec. III. There is an evolution of rounded maxima at elevated temperatures of a broad component into a two-component sharp plus broad line shape around T_n with the sharp component being typically 100 times narrower than the broad. This two length scale line shape is in turn dominated by the sharp component at low temperatures.

In contrast to the results from the specular reflection, scattering from those domains with a propagation wave vector lying in the surface plane of the sample (vis domains probed at the (102) reflection with propagation wave vector parallel to [100]) exists only in the form of a sharp response in both the $[h00]$ and $[00l]$ scan direction. Further, scattering is present only up to temperatures of 120.90 ± 0.05 K. On the scale of the response seen around the (003) peak there is no ''broad'' component either above or below the bulk phase transition for this reflection. The scans taken about (102) are illustrated in Fig. 6. The apparent lack of a broad component is significant since it indicates that the broad response seen in the specular (003) scans is unlikely to arise from thermodynamic fluctuations (which would be seen for all domains) but rather is a response particular to those planes which form the free surface. In addition, the data at the (102) position yields an estimate of the bulk phase transition temperature and the behavior of the sublattice magnetization on approaching T_n from below. In this sense we may use these data as a marker in unraveling the more complex behavior of the (003) specular reflection as discussed in Secs. III C and III D.

D. Energy dependence

In order to tune the spectrometer for resonance at the uranium M_{IV} edge, the sample was cooled well into the antiferromagnetic state (40 K), the spectrometer set to the position of the (003) antiferromagnetic Bragg peak and the incident x-ray energy scanned through energies close to the resonant scattering peak which was found to lie at 3.728 keV. These data, shown in Fig. 2, are in agreement with previous work on the isostructural compound UAs.[31–33] Careful scans at the points of antiferromagnetic reflection were also taken through the resonant energy at a sample temperature of 120.85 K. This temperature was chosen since

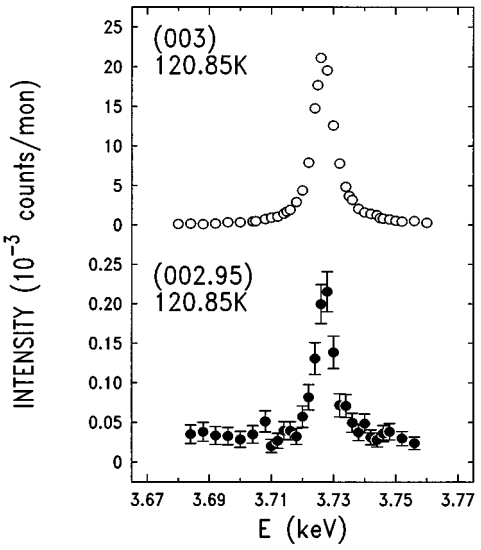

FIG. 7. Energy dependence of the resonant scattering at 120.85 K taken in the neighborhood of the (003) Bragg point scanning through the sharp and broad components, open circles and closed circles, respectively. The similarity with the results of Fig. 2 and Refs. 31–33 (in line shape and center) indicates that the signal is magnetic in origin for both components of the line shape. The error bars at (003) are smaller than, or of the size of, the open circles.

it exhibits the two-component line shape enabling us to verify the resonant nature of the scattering for both components under fixed sample conditions. In Fig. 7 it may be seen that the broad component (filled circles) does indeed show the same resonant behavior in energy as the sharp component (open circles) giving confidence that the two components of the line shape are both magnetic. In order to identify the individual components of the scattering (dipolar, quadrupolar, etc.) it will be necessary to carry out a full polarization study. Experiments carried out in UAs (Refs. 31–33 and 41) indicate that at the M_{IV} edge the dominant transition is electric dipole in nature and confirm the magnetic origin of the observed scattering. These conclusions may be transferred to UP assuming the uranium electronic configuration is similar.

E. Angular resolution

On account of the wide range of q space covered in the scans and the changing widths at least some consideration of the angular resolution must be taken. The resolution has three principal components associated with the spectrometer; the monochromaticity of the incident x-ray beam, the finite divergence of the incident beam upon the sample, and the finite acceptance angle of the detector. We exert no energy selection of the scattered photons except that afforded by the Bicron scintillation detector and the absorption in the sample to detector flight path both of which we take as energy independent over the energy range of interest (few eV at 3.728 keV). The sample contributes to the resolution principally through its mosaic spread. Taking the angles α and β, defined in Fig. 8, as independent random variables distributed about their mean value in Gaussian fashion gives an angular resolution function of the form

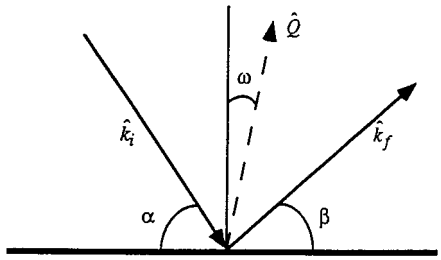

FIG. 8. Definition of the angles and geometry of the scattering plane as used in the expression for the resolution function. The surface is depicted by the heavy horizontal line in the figure. The direction q_z is parallel to the surface normal and q_x is parallel to the surface in the plane of the figure.

$$R(\alpha,\beta)=N\exp[-(\delta\alpha/\Delta\alpha)^2]\exp[-(\delta\beta/\Delta\beta)^2].$$

On transformation to the scattering plane coordinates (q_x,q_z) one obtains

$$R(\delta q_x,\delta q_z)=NJ\ \exp(-A_{xx})\exp(-B_{zz})\exp(-C_{xz})$$

with the coefficients A_{xx}, B_{zz}, C_{xz}, N, and J given in the Appendix. The presence of a cross-coupling term (C_{xz}) should be noted as this may give rise to extra width in the essentially sharp transverse scans in the presence of broad specular scans.

Finally, it is important to note that at the low incident energies used in this study (3.728 keV) the x-ray penetration depth into the sample is limited by absorption and may significantly restrict the number of atomic layers probed perpendicular to the surface in the ordered phase. To account for this the resolution function is convolved with a scattering function which contains explicitly within it the x-ray penetration depth (further discussion is given in the Appendix). The resulting line shape at a given temperature is simultaneously fitted to the data at both the specular (003) and off-specular (102) reflections in the two orthogonal directions parallel and perpendicular to the surface normal which lie in the scattering plane with just *one* intensity scaling constant which is fixed by the response at low temperatures. The out of scattering plane resolution is assumed sufficiently relaxed that it integrates over the scattering profile at all temperatures.

III. INTERPRETATION OF THE RESULTS

A. X-ray resonant magnetic-scattering cross section

Before commencing an analysis of the data we briefly summarize our assumptions concerning both the nature of the incident radiation and the x-ray resonant magnetic scattering cross section itself. First, the synchrotron x-ray source yields an inherently brilliant beam. The beam incident on the sample may be considered as an incoherent bundle of elemental coherent rays with coherence volumes typically 0.1–1 μm in dimension. This large dimension of the coherence volume is a primary result of the high brilliance of the x-ray source and can exceed the typical size of the magnetically ordered regions contributing to the diffracted signal from the sample. In such cases it may be necessary to con-

sider the scattered intensity as an incoherent sum of the individually diffracted elemental coherent rays rather than the Fourier transform of a (two-point) magnetic correlation function spatially averaged over the sample. Although this distinction is usually not made, under the implicit assumption of randomly phased scattering objects, it may become important in the vicinity of a phase transition and for phase transitions of a discontinuous nature where the nucleation and growth of phase-coherent islands of the ordered state may occur. As a concrete example consider a material with a magnetically ordered surface layer which supports a dendritic structure of magnetically transformed regions extending into a paramagnetic bulk. The dendrites will be phase coherent since they originate from a common surface layer.

The resonant x-ray scattering amplitude refers to a coherent two-photon process involving the excitation of an electron from a core state to an outer (magnetically polarized) energy level and its subsequent decay. In the ''fast collision'' approximation one assumes that the core hole liberated by photon absorption does not have time to propagate before the emission of the resonant photon and the concomitant refilling of the core level. This localizes the particle-hole pair (generalized magnetic fluctuation) and reduces the scattering cross section to the Fourier transform in time of a *two* site interference function summed over the coherence volume. The photon coherence length is normally sufficiently small that the resonant x-ray-scattering technique yields an approximation to a two-site instantaneous interference function and enables one to take a ''snapshot'' of the magnetic spatial correlations. The precise nature of the two-point function is determined from the conservation of angular momentum (order and nature of transition: electric or magnetic; dipole, quadrupole, mixed, etc.) and the harmonic order of the reflection concerned.[42] The resonant cross section coupled with a brilliant photon beam permits us to resolve weak signals and to define the diffraction profile with precision, this permits maximal separation of multicomponent line shapes.

B. Model cross section

In the overview of the experimental data, given in Sec. II C, Fig. 4 demonstrates the strongly anisotropic response for scans parallel and perpendicular to the surface normal around the (003) reflection. In particular, the specular scans have an extra scattering intensity in the region of, and above the transition temperature. This extra intensity is characteristically ''broad'' for scans parallel to the surface and ''sharp'' in the transverse cuts which suggests the formation of extended sheets of ferromagnetically aligned moments parallel to the sample surface which themselves are antiferromagnetically coupled, only a few layers deep, normal to the surface. In order to analyze this data we take the idea of formation of near-surface antiferromagnetic layers literally and introduce a simple model of layer formation in real space. The reason for the nucleation of the phase transition in the near-surface layers is unknown. Conceivably the cleavage of the sample induces an anisotropic strain in the near-surface region which, through the magnetovolume interaction,[43,44] favors near surface magnetism for one particular domain orientation. Alternatively, one may argue that the very presence of the surface allows for relaxation of stress and that through the magnetoelastic coupling a near-surface magnetization results. We note that intrinsic defects and inhomogeneities which were present in the bulk of the sample at the point of cleavage are not expected to be different from those below the cleaved surface, hence it would be difficult to invoke them as a source of local magnetization by themselves. Contamination from surface oxidation immediately prior to insertion in the displex may play a role. In this regard, our only control is to note that data taken on the same surface after a storage time of six months in a desiccator (10^{-2} Torr) is sensibly the same as that taken immediately after cleavage. The further analysis given below does not depend upon the microscopic origin of formation of magnetically ordered layers; we take this as a problem for future study.

As a preliminary model, we considered the specular scattering from a set of magnetic layers of uniform (temperature independent) extent parallel to the surface plane of the sample and of varying number normal to the sample's surface. On this assumption all calculations became one dimensional. The data were taken to represent the spatial Fourier transform of the instantaneous correlations of a set of ferromagnetic sheets coupled alternatively up and down in the direction normal to the surface of the sample. The model parameters were simply the number of layers perpendicular to the surface and their scattering moment. Results of this model on the isostructural compound UAs have been presented.[16]

In both this first model and the one to be developed below we make the approximation that the regions of antiferromagnetic order are terminated abruptly in space. The second approximation made is to assume that each incident coherent radiation volume scattering from the crystal samples the same distribution of antiferromagnetic layers in space. And finally that each incident coherent radiation volume is similar. Although these assumptions give rise to small oscillations in the computed cross section, they avoid additional sets of parameters to represent the decay lengths, a volume distribution function of antiferromagnetic layers and a distribution function of incident coherence volumes, respectively. The key result of our study, of an anisotropic near-surface magnetism giving rise to a two-component line shape, should not be affected by such considerations.

In this publication, we consider a slightly more sophisticated model than that used in Ref. 16 based on antiferromagnetically correlated planes of a temperature-dependent size. As in the first model, the number of antiferromagnetic planes is determined by the diffraction profile in the direction of the ordering wave vector. However, the spatial extent of the planes is now determined consistently from the scan transverse to the ordering wave vector. Since experimental data could only be taken along one of the two principal axes which lie transverse to the ordering wave vector we invoke the crystalline symmetry and infer a similar dimension for the unmeasured axis. Explicitly, in an ordered region the symmetry is tetragonal with the tetragonal axis parallel to the ordering wave vector. If, considering a specular scan by way of example, N_z is the number of antiferromagnetically correlated layers along the tetragonal axis and N_x is the measured dimension (in lattice units) of the layers from the transverse scan, we set $N_y = N_x$ in all calculations. The full scattering surface is computed as a function of N_x, N_y, N_z, and the sublattice polarization at each temperature and

convolved with the instrumental resolution function. From the resultant surface one projects out that cut relevant to the particular scan under consideration. The scans in orthogonal directions are coupled through the cross term C_{xz} inherent in the resolution function (the only way to avoid such a term is to arrange $\alpha=\beta$ *and* $\Delta\alpha=\Delta\beta$) and in this way the line shape in the q_x direction of the specular scans is broadened due to the finite extent of the antiferromagnetic diffracting region in the z (surface normal) direction.

Since we are unable to make reliable calculations of the absolute measured intensity of the resonantly diffracted beam, we scale the measured intensity at 77 K to the square of the effective moment reported by neutron diffraction in the literature at this temperature.[39,45,46] Caution must be exercised in interpretation since the energy ranges, wave-vector ranges and the coherence volumes covered by the respective experimental resolution functions in the x-ray and neutron experiments are very different. The scaling of the low-temperature moment amounts to the assumption that at these temperatures the diffracted intensity is dominated by the static (long-time average) sublattice magnetization and the presence of long-range order eliminates the problems posed by the different coherence volumes of the two radiation sources. At elevated temperatures, where such assumptions break down, we are on more delicate ground. It must be held in mind that the estimated value of magnetic moment is that appropriate to the instantaneous two-point correlation function and this is not necessarily equal to the equilibrium long-time average.

C. Application of the model to the specular scans

We now turn to the measured x-ray magnetic-scattering response around the (003) antiferromagnetic Bragg point taken on cooling. We divide the data into three temperature regimes according to line shape. A first low-temperature span below 120.5 K, a second transitional span from 120.5 to 121.1 K and a final high-temperature region above 121.1 K. These regions are characterized by a single sharp profile in the specular scan, a classic two-component line shape and a broad profile respectively (see Sec. II C and Fig. 5).

Starting at low temperatures the magnetic peak is, over its central portion, dominated by the angular resolution function. The specular and transverse cuts differ in width by a factor of 2 in this regime and this is picked up by the relative widths of the resolution function which scale, respectively, as the sine and cosine of the half-scattering angle (for further discussion see the Appendix). Away from the central position the Lorentzian-like tails in the specular scans are dominated by the finite penetration depth. In a simple manner this may be understood as the exponential decay of the incident and scattered beams due to absorption which yields, on Fourier transformation, a Lorentzian form in reciprocal space. In the transverse direction extended tails are also seen. These arise from the finite domain size and/or the transverse coherence length of the incident radiation. From the low-temperature data we then set the effective angular resolution, the effective penetration depth into the sample and obtain an estimate of the domain size or transverse coherence length. The numerical values of these parameters are given in the Appendix under the discussion of the resolution function. On

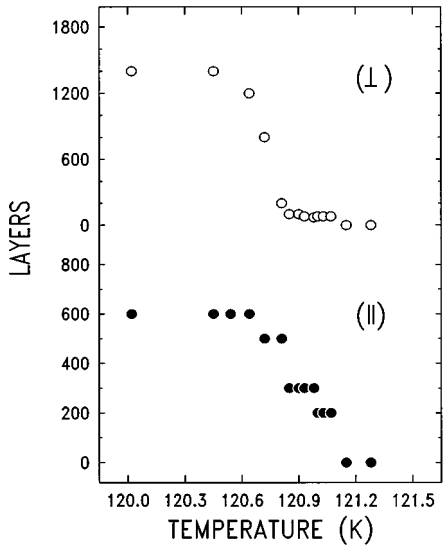

FIG. 9. Thermal evolution of the number of magnetic layers of the bulk response deduced from the width (and intensity) of the measured response in the directions parallel and perpendicular to the ordering wave vector around the specular (003) Bragg point. The layers are in units of the chemical unit cell. The estimated error in the number of layers is of the order of 10%.

heating the scattered intensity starts to fall as evidenced in the plots of integrated intensity (Fig. 3). Less obvious are the changes in line shape. Since the diffracting objects remain relatively large until very close to the transition the FWHM is dominated by the angular resolution and only by looking in detail at the tails of the scattering may the changing sizes of the coherently diffracting regions be seen. Once the changing size of the diffracting regions is taken into account one may estimate the effective scattering moment (see also discussion in Sec. IV C).

Empirically, the scans start to become noticeably broader at temperatures above 120.5 K, Fig. 5. This arises from two effects. First, the size of the diffracting objects themselves become smaller giving rise to a width in the sharp component greater than that contributed by the angular resolution. Secondly, the development of near-surface magnetism occurs which gives rise to a broad component in the specular profile. The thermal evolution of the number of magnetically ordered layers in the bulk magnetic phase is given for directions parallel and perpendicular to the ordering wave vector in Fig. 9. Experimental transverse cuts through the scattering surface away from the position of maximum intensity were made and compared favorably with the calculated response within the model function given. A typical pair of scans taken in the vicinity of the phase transition and exhibiting the two component line shape in the longitudinal direction are given in Fig. 10. The model function is able to reproduce the width and intensity in the directions both longitudinal and transverse to the ordering wave vector. The broadening raises a problem in the definition of T_n. Direct plots of inverse linewidth against temperature would imply the phase transition is signaled by an onset of ''long-range order'' (resolution limited scattering profile) occurring below T_n as determined from intensity measurements (see, for example, Ref. 13). Within the model used the interpretation is rather of

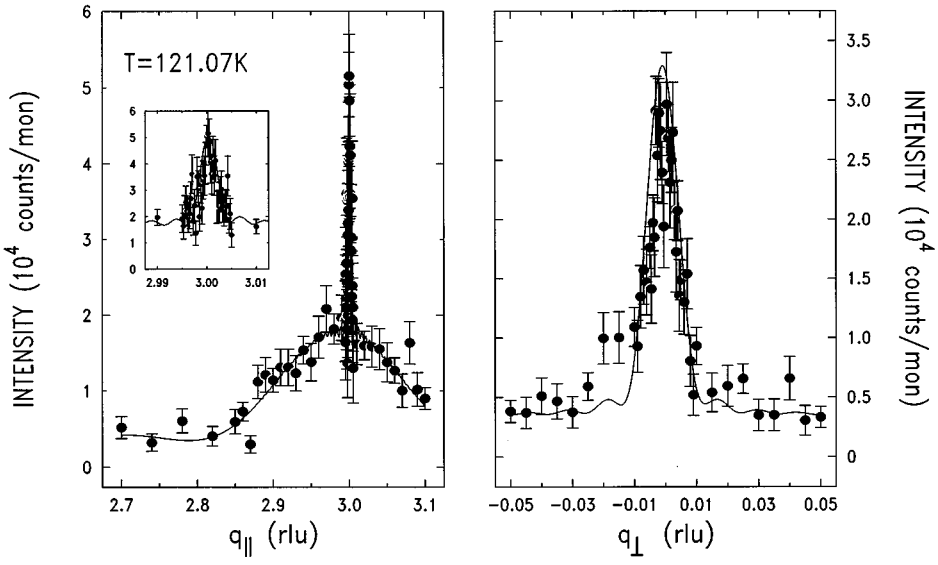

FIG. 10. Data and fits to the model function in the two length scale regime. The inset on the longitudinal scan (parallel to the ordering wave vector) shows the sharp component on an enlarged scale. The small oscillations in the fitted functions come from the single component distributions used for the surface and bulk layers as discussed in the text. The maximum of the response occurs just off the low-temperature Bragg position in the specular direction; for this reason the transverse cut is less intense in its peak height than the longitudinal cut. The displacement has been put into the model calculation.

a falling size of domain on approaching T_n. Further problems occur with differences between the specular and off-specular response, and we give a working definition of T_n in Sec. III D below.

Above 120.5 K an additional broad feature associated with near-surface magnetism arises in the scattering profile. The evolution of the number of magnetically ordered layers in this near-surface magnetic phase is given for the directions parallel and perpendicular to the ordering wave vector in Fig. 11. Again, as in Fig. 9, we note the extreme anisotropy of the response parallel and perpendicular to the ordering wave vector. Interestingly, the inferred moment associated with the near-surface magnetism increases from the bulk value at 120.5 K to a broad maximum, with a value close to the free-ion moment, and starts to decay again above 121.1 K. The abrupt fall at 121.1 K is followed by a plateau extending to temperatures as high as 130 K, (Fig. 12). Further discussion of the evolution of the ordered magnetic moment and its interpretation within a simple Ginzburg-Landau model are given in Sec. IV.

D. Application of the model to the *off*-specular scans

As observed in Sec. II C the scattering at the (102) reflection is much simpler than that around the (003) Bragg point. It is also much weaker. This loss of intensity at low temperatures is accounted for by the proposed resolution function given the assumption of an equal domain population. The typical difference in intensity and line shape of the (003) and

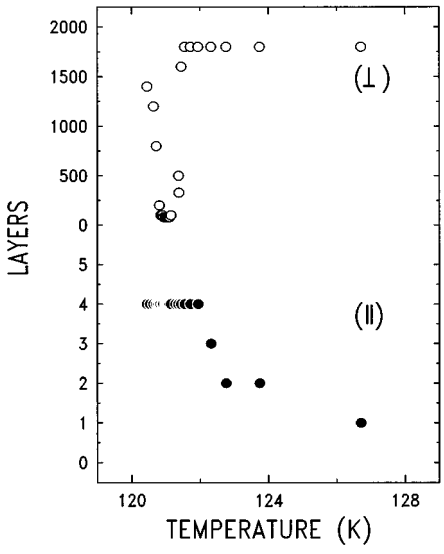

FIG. 11. Thermal evolution of the number of near-surface magnetic layers deduced from the width (and intensity) of the measured response in the directions parallel and perpendicular to the ordering wave vector around the specular (003) Bragg point. The layers are in units of the chemical unit cell. At and above 130 K there exists a weak intensity over and above that seen at 200 K; however the uncertainty in the line shape is too great to allow an unambiguous analysis.

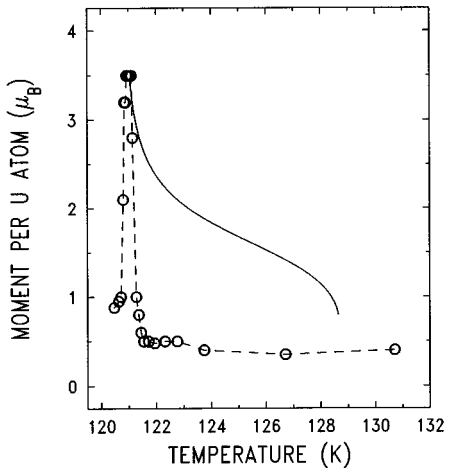

FIG. 12. Thermal evolution of the effective near-surface sublattice magnetization per uranium atom deduced from the model scattering function introduced in Sec. III. The peaking of the moment in the vicinity of the phase transition may be understood in terms of an extended Ginzburg-Landau model of Sec. IV. The solid line is the expected temperature variation of the Ginzburg-Landau surface layer moment using parameters derived in Sec. III. The estimated error in the value of the effective moment is of the order of 10%.

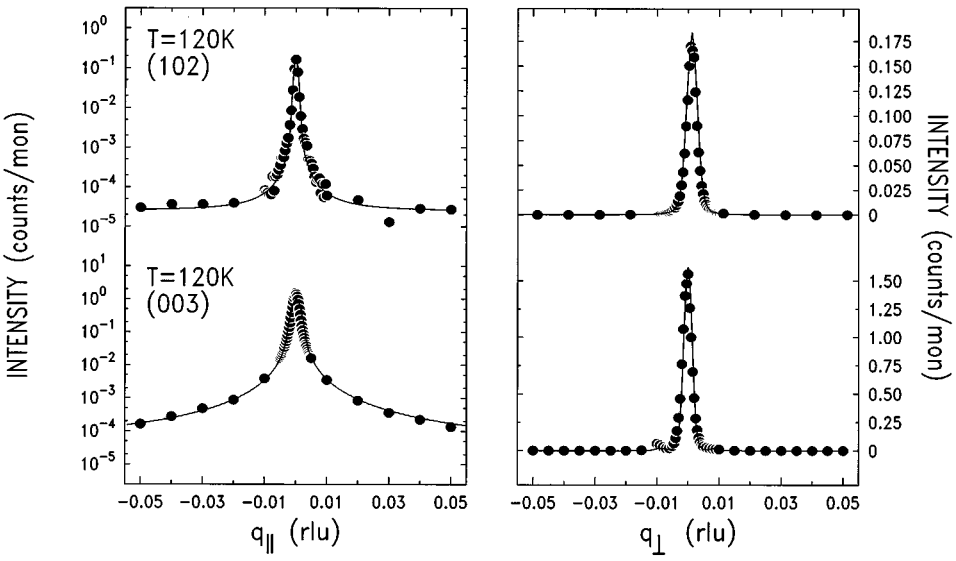

FIG. 13. Contrasting intensities and line shapes shown for scans taken in the specular (003) and off-specular (102) reflections in the antiferromagnetic phase. The longitudinal scan is along the direction lying parallel to the sublattice magnetization in the given domain. This is the [00*l*] direction for the specular (003) reflection and the [*h*00] direction for the (102) off-specular reflection. The transverse scan directions lie in the scattering plane and are orthogonal to the given longitudinal directions. The solid line is a result of a fit given by the model described in the text with one scaling parameter for the vertical axis.

(102) reflections in the ordered phase is shown in Fig. 13. In each case the longitudinal scan is parallel to the magnetic propagation vector ([001] for the (003) reflection and [100] for the (102) reflection) and the continuous line is the result of a fit to the model. The transverse scans are perpendicular to the ordering wave vector and in the scattering plane. At both reflections the data presented has been taken on cooling; as noted in Sec. II B there is no observable hysteresis in up and down temperature sweeps. In the analysis of the specular and off-specular scans there is just one scaling constant for all scans. The sublattice moment, sizes of diffracting regions and domain fraction are then determined consistently from all data at a given temperature. Since the data for the two domain orientations were taken on different heating and cooling cycles this procedure supposes that the experimentally sampled domain fraction is approximately independent of sample history. This was confirmed by the near reproducibility of data taken on the same sample surface in two separate experiments and is a result of the averaging given by the large incident beam size (of order one millimeter) in comparison with a typical domain size (of order micrometer). As illustrated in Fig. 14(a), the fraction of off-specular domains goes to zero at a temperature of 120.9 K as does the sublattice moment [Fig. 14(b)]. We assign this temperature T_n (of the bulk). In contrast, the specular reflections which give evidence of continued bulk order up to temperatures of 121.1 K are taken to be extraordinary. The difference is illustrated in Fig. 15 where at 120.92 ± 0.01 K, for scans along the ordering wave vector, a sharp response is observed for the specular (solid circles) in contrast with the off-specular (open circles) where no observable response is seen. This then suggests that the different domains, specular and off-specular, have significantly different physical behavior above 120.9 K, an issue which is discussed further in Sec. IV C.

IV. DISCUSSION

A. Overview

From the model interpretation of the observed diffraction profiles the following picture of the antiferromagnetic phase transition in UP arises: starting at low temperatures in the ordered phase antiferromagnetic domains occur with approximately equal probability. The bulk sublattice magnetization evolves in a smooth manner to around 120.8 K, whereafter the specular and off-specular reflections have quite different behaviors as detailed in Secs. III C and III D. Above 120.5 K, one has evidence of a near-surface sublattice magnetization with an effective moment substantially different from that observed in the bulk which occurs exclusively for that domain having its ordering wave vector parallel to

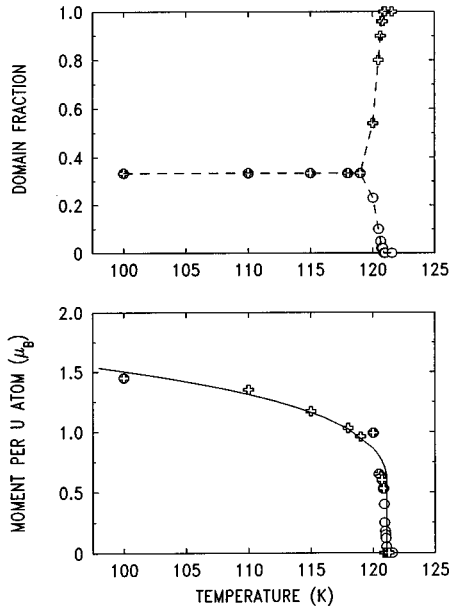

FIG. 14. Top panel: The domain fraction as extracted from the fits to the model of Sec. III. The open crosses and circles represent the specular and off-specular fractions, respectively. The dashed line is a guide to the eye. Bottom panel: The overall temperature dependence of the effective moment per uranium atom (scaled to the low-temperature value) for the specular and off-specular scans given by the crosses and circles, respectively. The solid line is a fit to a first-order Ginzburg-Landau model of the form f_b given in Sec. IV. The parameters used are $T_c = 120.8$ K, $T^* = 121.1$ K, and $m^* = 0.64\mu_B$ per uranium atom.

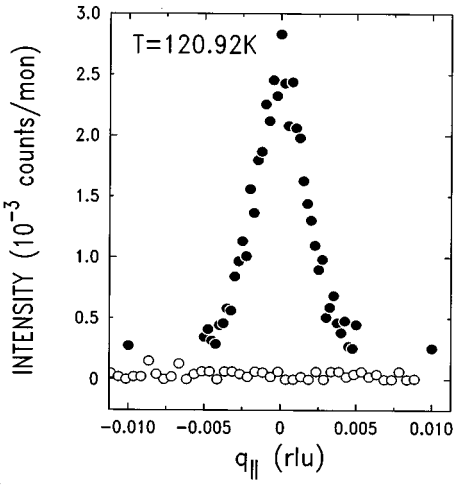

FIG. 15. Longitudinal scans along the ordering wave vector in the temperature regime between T_c and T^* for both the specular and off-specular directions. Only the specular reflection (filled circles) shows any response in this temperature interval. This response appears to be nucleated by the presence of near-surface magnetic layers which occur exclusively for domains orientated with their ordering wave vector along the free surface normal.

the surface normal. Both the near surface and bulk polarized regions are of similar lateral dimensions, giving an image of continuous blocks of antiferromagnetic layers extending down from the surface into the bulk. Below 120.9 K these blocks are interspersed by those of the other domains. The unusual temperature dependence of the near-surface magnetization, its existence to temperatures as high as 130 K and the peaking in intensity occurring in the vicinity of the bulk phase transition lead us to consider a general analysis of surface magnetism at phase transitions of a discontinuous nature.

We discuss a mean-field Ginzburg-Landau theory and consider separately two effects, both of which indicate the possibility of having a surface ordering occurring above the bulk phase transition. The simple Ginzburg-Landau approach is open to the criticism that it is known to yield incorrect predictions near critical points; however, in many cases it does yield insight into the qualitative nature of the phase diagram and may give some guidance to the underlying physical effects. It is in this spirit that we use it here. The first approach is to continue to ignore the surface explicitly in as much as the breaking of translational invariance is neglected, while emphasis is put upon the magnetoelastic interaction and relative strains occurring in the surface and bulk layers. The second approach is to focus precisely upon the perturbations to the order parameter induced by the breaking the spatial translational invariance. In the concluding section we comment briefly on how the breaking of translational invariance by point and line defects may play a role in the more general case.

B. Surfaces ignoring the breaking of translational invariance

First, we ignore the explicit breaking of translational invariance imposed by the surface. The effect of the free surface is to allow lattice relaxation; this effect will be more pronounced the more disordered the surface in the sense that one may imagine blocks of material able to relax with minimal constraint both parallel and perpendicular to the average sample surface. A minimization of the free energy of the coupled order-parameter system of the magnetic and strain degrees of freedom is then required. In the classic case, explored in detail by Bean and Rodell,[43,44] such a minimization is well known to shift the transition temperature relative to that occurring in the strain free but magnetically or otherwise stressed configuration. In particular, such a minimization will always reduce the coefficient of the quartic term in the free energy through the magnetoelastic coupling effect. The assumed positive quartic term which gives the mode cross coupling depresses the phase transition temperature from its independent mode mean-field value. The depression of the temperature of the phase transition has been calculated for example, in a quantitative manner, for a series of incipient and weakly magnetic metals.[47–50] The reduction of the effective coefficient of the quartic term through the magnetoelastic effect, reducing as it does the mode coupling, leads to an enhancement of the renormalized phase transition temperature in the stress-free regime. This is different from an enhancement of T_n which is equally possible on the application of hydrostatic or uniaxial stress where the appropriate free energy to be minimized is not that of a stress-free system. Eventually, in the case of extreme reduction of the quartic coefficient from a positive to a negative value one may imagine driving the phase transition first order introducing the possibility of passing through a tricritical point. Thus we have an intrinsic mechanism for (near) surface ordering above the bulk phase transition for systems in which the coupling of fluctuations and internal stresses plays a significant role (for a related discussion see, e.g., Ref. 1). Clearly, coupling to any other parameter in a similar fashion will work; strain just seems most obvious. Alternatively, one may suppose that sample dependent stresses, for example, induced by cutting or other surface treatments, yield an enhancement of T_n in the near-surface region in an analogous manner to the application of hydrostatic or uniaxial stress. However it is not clear that internal stresses would necessarily always act in the correct direction and be of sufficient magnitude such as to be able to give the measured enhancement of T_n. Further, the volumetric distribution of stress in the near surface, and hence T_n, would have to be such as to match the observed evolution of scattering intensity. The explicit first-order nature of an idealized transition and the disruption of translational invariance by the surface are our next concern.

C. Surfaces with the breaking of translational invariance

We consider a scalar order parameter to represent the sublattice magnetization and set up a coordinate system with the sample being supposed semi-infinite in the x,y plane and having the z axis running from 0 at the sample free surface to infinity into the bulk.[51] The scalar nature of the order parameter does not admit the general vector form of a magnetic problem, but in our case of extreme uniaxial anisotropy in a given domain is taken as a starting point for discussion with the caveat that the true vector nature of the problem may eventually lead to significant differences.[47–50] The inclusion

of the surface breaks the translational invariance of the problem and we anticipate having to add two terms to the free energy. The first is to take care of the spatial gradient of the order parameter perpendicular to the surface $m=m(z)$ implied by the lack of translational invariance. The second is a term to mimic the effect of the open surface, essentially to signal out the surface layer. This is taken in the spirit of simple Ginzburg-Landau theory to be proportional to the square of the surface magnetization and is labeled f_1. We consider a free energy of the following form:

$$F=\int_0^\infty dz(f_b+f_s),$$

where the free energy density has been arbitrarily broken into two pieces for ease of calculation. The term f_b is chosen to yield a first-order transition with the coefficients a, b, and d positive. To accommodate the gradients introduced by the surface the sublattice magnetization density is generalized to $m=m(z)$ giving

$$f_b=\frac{a}{2}m^2-\frac{b}{4}m^4+\frac{d}{6}m^6,$$

with f_s the surface-induced contribution of explicit form

$$f_s=\frac{c}{2}\left(\frac{dm}{dz}\right)^2+f_1\delta(z),$$

$$f_1=\frac{a_s}{2}m^2,$$

where $a=a(T)$ is the primary temperature-dependent parameter of the theory. The bulk free energy has two characteristic temperatures of interest. The first is contained in the supposed linear variation of $a(T)$ about T_c, $a(T)=a_1(T-T_c)$; at and below T_c the stable state is one of finite sublattice polarization. The second temperature comes from the point of instability where the free energy passes with its minima at finite sublattice magnetization through zero at $T=T^*$. We label the magnetization density at this point m^*. Between T^* and T_c a metastable state pertains in which temperature interval the system may pass discontinuously from a paramagnetic to ordered state.

The model works in the following manner. At a given temperature above T^* the stimulating term $f_1\delta(z)$ raises the surface layer to an (arbitrary) magnetization. Physically, this may represent the presence of surface disorder or other effects as considered in Sec. IV B. Provided this surface magnetization is greater than m^*, the system will support a *spatially extended* decay of magnetization density into the bulk. Roughly speaking this new length scale arises in the following manner. Starting from the surface where the free energy has a large negative contribution, the minimum in f_b traps the system at finite magnetization density over a distance given by the energy cost incurred by the gradient term contained in f_s. This allows for a delocalized near-surface magnetism on a length scale which diverges at T^*, even though the stimulating term is strictly localized at the surface. The divergence at T^* corresponds to a bulk transition in the metastable regime with the surface layer playing the role of a nucleation center.

To expand upon these descriptive ideas we search for the functional form of $m(z)$ which renders the free-energy stationary; one derives the Euler-Lagrange equation:

$$c\left(\frac{d^2m}{dz^2}\right)=\frac{df_b}{dm} \tag{1}$$

and the boundary condition

$$\frac{df_1}{dm}=c\frac{dm}{dz} \tag{2}$$

evaluated at $z=0$.

Equation (1) is integrable (cf. Newton's law) to give

$$\frac{c}{2}\left(\frac{dm}{dz}\right)^2=f_b(m)=\text{const}. \tag{3}$$

We are primarily interested in the occurrence of near-surface magnetization when the bulk is paramagnetic, this gives the boundary condition that at large distances from the surface $m(z)$ tends to zero. As may be seen from Eq. (1), a monotonic f_b as a function of m, characteristic of a continuous phase transition above T_c, cannot yield an extended region of near-surface magnetism. At most one may arrive at a decaying magnetization starting from an assumed magnetic surface layer given by a negative value of a_s. Such a model has been explored and is incompatible with our data sets. Extended or delocalized near-surface magnetism existing in the bulk paramagnetic phase implies f_b exhibiting a dip as a function of m to yield a point of inflection in $m(z)$ [given by Eq. (1)] coupled with a negative value of a_s.

Explicitly solving Eqs. (1) and (2) for temperatures above T_c:

$$m(z)^2=m^{*2}\left(\frac{T-T_c}{T^*-T_c}\right)\left[1+\sqrt{\frac{T-T^*}{T^*-T_c}}\sinh(2z\kappa+AS)\right]^{-1},$$

where the inverse correlation length is given in the normal manner as

$$\kappa=\sqrt{\frac{a}{c}}$$

and

$$AS=a\sinh\left(\frac{\left(\frac{m^*}{m(0)}\right)^2[(T-T_c)/(T^*-T_c)]-1}{\sqrt{(T-T^*)/(T^*-T_c)}}\right),$$

with $m(0)$ being the surface magnetization.

At temperatures above T^* solving Eqs. (2) and (3) one obtains

$$m(0)=m^*\sqrt{1+\sqrt{\frac{T_s-T}{T^*-T_c}}},$$

where the effective surface transition temperature

$$T_s=T^*+\frac{a_s^2}{a_1c}.$$

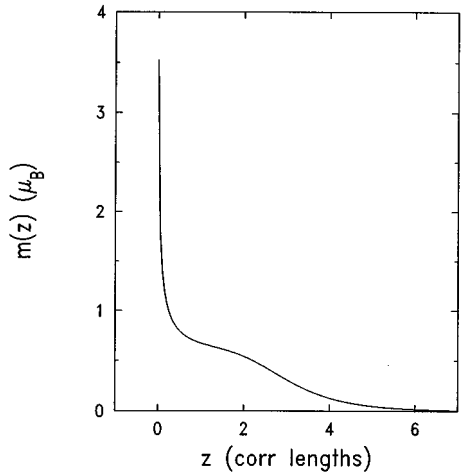

FIG. 16. Profile of $m(z)$ calculated in the vicinity of T^* in terms of the reduced length scale (the correlation length). Comparison with the experimental data indicates a correlation length in the region of 7 Å.

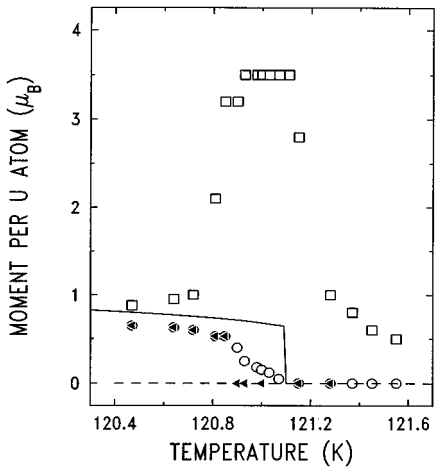

FIG. 17. Detailed temperature dependences of the near-surface moment (open squares), the specular bulk response (open circles), and the off-specular response (filled triangles). The solid line is from a first-order Ginzburg-Landau model of the form f_b used in Fig. 14 with the same parameters. The deviations of the bulk responses from the solid line are discussed in Sec. IV C. The near-surface magnetic moment falls to merge with the bulk value starting around T_c, below which temperature a more sophisticated model is required.

The possibility to have a plateaulike region in $m(z)$ at a given temperature depends on the quantity AS being negative and the spatial extent is given in magnitude as AS times the correlation length. From the explicit equation for AS this is seen to imply $m(0)$ being greater than m^*. Further, the closer T is to T^* the more negative AS becomes and hence the larger the region of delocalized or near-surface magnetization. This then mimics the behavior found in our analysis of the data. The parameters T_c and T^* we estimate from the behavior of the bulk (003) and (102) magnetization density to be 120.8 and 121.1 K, respectively. This leaves the scaling parameter m^*, the value to which the sublattice magnetization jumps at T^* in those regions which transform. This is estimated to be approximately $0.64\mu_B$ per uranium atom from the temperature dependence of the magnetic moment derived in Secs. III C and III D. A profile of $m(z)$, calculated in the vicinity of T^*, is sketched in Fig. 16. From the spatial extent of the near-surface layers estimated within the model of Sec. III B, which is approximately 25 Å near T^*, one obtains the correlation length from this figure to be around 7 Å which corresponds well with that estimated by independent neutron-scattering measurements for temperatures above T^*.[37]

Application of this formalism to our results is shown by the solid line in Fig. 14(b). Overall, the form of f_b accounts reasonably well for the observed temperature dependence of the magnetic moment inferred in Secs. III C and III D. In detail, Fig. 17 indicates that the sublattice moment of the off-specular (102) domain (filled triangles in figure) jumps at a value close to the T_c of the Ginzburg-Landau model. This suggests that the off-specular domains are not significantly nucleated above this temperature (120.8 K). Also notable is that until temperatures below 120.5 K the estimated moment is lower than the theoretical curve. This may be accounted for by the analysis (Sec. III) since the size of the diffracting regions in the dimension transverse to the wave vector of propagation is smaller than the beam coherence area at these temperatures and we (arbitrarily) set the number of such diffracting objects to the ratio of the beam coherence area to their size (its maximum value). If the number of randomly phased diffracting objects is less than this theoretical maximum, the moment assigned would have to be increased to yield the observed intensity in agreement with the Ginzburg-Landau estimate. For the specular (003) scans above T_c (open circles in Fig. 17) there is an ever decreasing moment up to T^*. To satisfy the extrapolated Ginzburg-Landau value of moment one would infer that the nucleation probability, and hence the number of transformed regions, is falling rapidly on approaching T^* due to an increasing free energy barrier.

Although formally outside our starting Ginzburg-Landau model, an increase in near-surface moment on approaching T^* from above may be mimicked by assuming a temperature dependence of the Ginzburg-Landau stiffness parameter c. Taking the effective surface moment to be limited to the free-ion value, and c to vary as $(T-T_c)$ with a value of m^* from the calculation in the ordered phase the solid line is obtained in Fig. 12. This displays a characteristic upturn in the vicinity of the bulk phase transition and an estimated T_s of 130 K in rough agreement with the observation. As the parameter c becomes small the moments become decoupled. This near criticality of the stiffness in addition to that of the susceptibility appears to be an important aspect of strongly correlated systems.[52] On further cooling below T_c the surface moment falls whereafter it merges with the bulk.

In a more general framework one may obtain a delocalized order parameter in the paramagnetic state whenever the free energy admits a dip at finite magnetization, provided there is some term analogous to f_1 locally to surmount the free-energy barrier and provide the nucleation center. This forcing term may be static or dynamic; importantly it does *not* have to exhibit a long-range field itself, the length scale comes, as in the case of spontaneous fluctuations, from the functional minimization of the free energy. Examples of static forcing terms are point, linear, or planar defects and

spontaneous thermodynamic fluctuations or mobile defects provide dynamic ones. Since in our experiments we only see the two-component line shape for the specular scans of those domains having the ordering wave vector parallel to the surface normal we assign the forcing term in our discussion to a planar defect in some way associated with the surface. Such equilibrium models have nothing to say on dynamic formation of magnetic surface layers and, as emphasized, x-ray measurements cannot at this stage eliminate such processes. We further note that in the vicinity of a phase transition we may anticipate modifications in line shape arising from changes in the long-range nature of the magnetic two-point correlation function[4] corresponding within a Ginzburg-Landau formulation to temperature-induced modulations of the stiffness coefficient (c) above. These variations may give rise to two-component line shapes even for continuous transitions in infinite media.

V. CONCLUSION

Before summarizing our results we pause to stress a difference of detail apparent between the interpretation of our results and those previously reported. In the latter, the two length scale diffraction profile is usually taken to exist only at temperatures *above* the (nominal) bulk transition identifying the anomalously sharp response with (a pretransition of) the near-surface layer and the broad response with the normal thermodynamic fluctuations. Indeed the temperature at which the sharp linewidth becomes resolution limited is often taken as a definition of T_n. UP and UAs are experimentally distinct from other materials studied to date such as Ho,[5] UO_2,[2] and NpAs (Ref. 3) in having a highly anisotropic line shape. In our data the manifestly broad response along the specular direction has been shown to be associated with the near surface and the two length scale diffraction profiles with a region of coexistence of surface and bulk (ordered) magnetism.

The model introduced in Sec. IV may be generalized in several ways. First, as already noted, if the transition is discontinuous terms other than the free surface may act to provide the necessary nucleation center for delocalized magnetism. Secondly, in the vicinity of a continuous phase transition strong fluctuations renormalize the free energy,[49,50,53,54] and may provide the necessary change in free energy to enable the local formation of delocalized near-surface magnetism. Finally, we note that a spatially modulated order parameter may be susceptible to the formation of similar pseudo-long-range order even for a continuous phase transition in the presence of point defects. All such mechanisms would yield, in the region immediately above T_c, finite but long-range order (the sharp component) which increases in spatial extent with lowering temperature. Within the framework outlined in Sec. IV the sharp length scale would be expected to diverge as some increasing multiple of the thermodynamic correlation length, ζ_c, on approaching T_c; that is it will diverge faster than ζ_c as observed. Further, the intensity associated with the second length scale will diverge with an exponent characteristically faster than that of the thermodynamic fluctuations, since the observed intensity of the second length scale would be driven both by an increasing correlated moment and an increasing number of nucleated sites. The lifetime of the extended spatial order is anticipated to be greater than or of the magnitude of its stimulus (see discussion in Sec. IV).

Our primary experimental result is the existence of a two-component line shape for the specular (003) reflection in the vicinity of the paramagnetic to antiferromagnetic phase transition in UP. While appreciating that since we measure a spatial Fourier transform we cannot prove that the broader of the two components is uniquely associated with the near-surface region, the analysis given makes it plausible. It is possible, through a detailed analysis of the scattering, to identify this antiferromagnetic near-surface phase at temperatures as high as 10 K above T_n. The coexistence of this phase with the incipient bulk phase is deemed responsible for the observed two-component profile in the vicinity of the bulk phase transition. The building blocks of the antiferromagnetic structure are ferromagnetically aligned sheets of sublattice magnetization of temperature-dependent spatial extent which are themselves antiferromagnetically coupled.

The second observation is that the bulk phase transition propagates as a two-stage process for the domains involved in the (003) specular reflection. There is an initial growth of antiferromagnetic order into the bulk of the sample from the near-surface layers associated with this specular reflection followed by the simultaneous growth of the two orthogonal domains, which have their moments lying in the surface plane, marking the start of the bulk phase transition. At temperatures just above T^* the transverse extent of the near-surface layers involved in the specular (003) reflection falls dramatically from its high-temperature (resolution limited) value, Fig. 11, and then picks up during the growth stage of long-range order. It remains an interesting question to understand this dissolving of initial (pseudo) long-range order of the near-surface layers on approaching the bulk phase transition and its regrowth. At low temperatures the measured domains, located in the near-surface volume, appear to be approximately equally populated in agreement with supplementary neutron-scattering investigations on the bulk of the same crystal.[37] It would clearly be of great interest to make detailed experiments both on a (polished/etched) smooth surface in addition to the reported experiments which were performed on a cleaved surface and on surfaces exhibiting different crystallographic planes. Given the cubic rocksalt crystal structure and the natural cleavage planes the above proposed transition (Sec. IV C) may commonly take place in such materials.

In addition to the above discussed precursor phase, neutron-scattering data indicates the formation, in the bulk, of (dynamic) antiferromagnetically correlated sheets, just a couple of layers deep, for all three domains at temperatures above and extending just into the bulk phase transition. We suggest that these may arise in the normal way from spontaneous fluctuations in the free energy (not large enough to surmount the barrier) with a spatial magnitude given by the thermodynamic correlation length. One thereby identifies, in general, three length scales in the discontinuous phase transition. These length scales, in ascending order, are those of thermodynamic correlations, the near-surface correlations, and the bulk correlations. The presence of highly anisotropic layers and a short thermodynamic correlation length facilitates the separation of such contributions, one or more of

which may become merged into another in the presence of more isotropic and longer ranging correlation lengths. In a more general way it may be useful to consider a distribution of active length scales in a given problem, here we approximate this distribution at each temperature by a singular value characteristic of each of three regimes. An analysis of the scattering profiles occurring in these more general cases is dealt with elsewhere.[42]

ACKNOWLEDGMENTS

We thank P. Burlet for making his UP sample available to us for this study and M. Altarelli and F. de Bergevin for illuminating discussions. S.L. and N.B. would like to thank the European Union for the HCM awards which made this work possible including work carried out under Grant No. CHRXCT93-0135. Work performed at Brookhaven National Laboratories is supported by the US-DOE under Contract No. DE-AC02-76CD00016.

APPENDIX: ANGULAR RESOLUTION

Following the nomenclature of Fig. 8 we express the experimental resolution function in terms of the angular variables α and β and their deviations $\Delta\alpha$, $\Delta\beta$. Three principal components are associated with the spectrometer; the monochromaticity of the incident x-ray beam, the finite divergence of the incident beam upon the sample, and the finite acceptance angle of the detector. We assume that the incoming and outgoing angular deviations are uncorrelated and no energy selection of the scattered photons over the energy range of interest (few eV at the resonant energy of 3.728 keV). The sample contributes to the resolution principally through its mosaic spread and possibly by its finite size for a small incident beam. Taking the incident monochromaticity, angular divergence, and sample mosaic together we define an effective incident angular divergence $\Delta\alpha$ in the vertical plane. In the same plane for open detector slits at a distance l from the sample and an illuminated sample of length s we have an outgoing divergence approximately given by $\Delta\beta = \sqrt{\{\Delta\alpha^2 + [(s/l)*\sin\beta]^2\}}$. For an incident beam of height w smaller than the sample length, s is to be replaced by $w/\sin\alpha$. We take α and β distributed about their mean value in Gaussian fashion yielding an angular resolution function

$$R(\alpha,\beta) = N \exp[-(\delta\alpha/\Delta\alpha)^2]\exp[-(\delta\beta/\Delta\beta)^2],$$

with a normalization

$$N = (\pi\Delta\alpha\Delta\beta)^{-1},$$

for the case where the slits are sufficiently wide open not to cut the outgoing beam. On transformation to the (q_x, q_z) coordinate system

$$R(\delta q_x, \delta q_z) = NJ \exp(-A_{xx})\exp(-B_{zz})\exp(-C_{xz}),$$

with

$$A_{xx} = \{\cos^2(\beta)/(\Delta\alpha)^2 + \cos^2(\alpha)/(\Delta\beta)^2\} \times [\delta q_x/(k_0\sin(2\Theta))]^2,$$

$$B_{zz} = \{\sin^2(\beta)/(\Delta\alpha)^2 + \sin^2(\alpha)/(\Delta\beta)^2\}[\delta q_z/(k_0\sin(2\Theta))]^2,$$

$$C_{xz} = \{-2\sin(\beta)\cos(\beta)/(\Delta\alpha)^2 + 2\sin(\alpha)\cos(\alpha)/(\Delta\beta)^2\} \times [\delta q_x/(k_0\sin(2\Theta))][\delta q_z/(k_0\sin(2\Theta))],$$

$$J = [k_0^2\sin(\alpha+\beta)]^{-1},$$

where θ is the Bragg angle.

The outgoing angular divergence is given approximately by the gap of the slits in front of the detector. This gives $\Delta\beta = 0.002$. From the low-temperature scans we set $\Delta\alpha = 0.0004$. The wave vector k_0 is given by the resonant energy and the angles α and β from the conservation of momentum. The effective penetration depth is in the region of 1200 Å and the transverse coherence/domain size is of the order of 1 μm.

At the low incident energies used in this study the x-ray penetration depth into the sample is limited. Since the attenuation depends on the actual scattering path length, that is, the angles α and β *and* the active scattering depth we compute it directly in the effective scattering function $S(q_x, q_z)$ rather than in the resolution function. It is of interest that the exponential decay of beam intensity with path length gives an identical form (with opposite sign) to the resolution as that obtained by considering a rough surface with an exponentially depleting number of layers.[55] The two effects may work one against the other to yield spurious estimates of both surface roughness and absorption coefficients. We work in large scattering angle geometry and ascribe our measured effects to an effective absorption depth.

The scattering amplitude f appropriate to the model function of Sec. III and from which $S(q_x, q_z)$ is constructed is taken to have the following form:

$$f = \sum_r M_s(\mathbf{r}) e^{i\mathbf{q}\cdot\mathbf{r} - \mu z} + \sum_r M_B(\mathbf{r}) e^{i\mathbf{q}\cdot\mathbf{r} - \mu z}$$

where M_S and M_B are the effective surface and bulk sublattice magnetization densities, respectively. The position vector $\mathbf{r} = (x,y,z)$ has directions x and y in the sample surface plane and z running from 0 at the sample free surface to infinity in the bulk. The scattering wave vector is equal to $\mathbf{q}$ and μ is the effective inverse penetration depth given by

$$\mu = \mu_0\left(\frac{1}{\sin\alpha} + \frac{1}{\sin\beta}\right).$$

Corrections to the simple Fourier-transform relationship between the object and the diffraction profile used in the analysis are generated by the nonplanar nature of the diffracted wavelets. Such effects are anticipated to become important when the dimension of the object giving rise to coherent diffraction exceeds the first Fresnel zone as subtended at the detector.[56] In the experimental geometry this would correspond to a coherent scattering object approximately 30 μm in dimension. This is much longer than the typical incident beam coherence length, excluding this as a source of error in the analysis.

[1] M. Altarelli, M. D. Núñez-Regueiro, and M. Papoular, Phys. Rev. Lett. **74**, 3840 (1995).
[2] G. M. Watson, B. D. Gaulin, D. Gibbs, G. H. Lander, T. R. Thurston, P. J. Simpson, H. J. Matzhe, S. Wang, M. Dudley, and S. M. Shapiro, Phys. Rev. B **53**, 686 (1996).
[3] S. Langridge, W. G. Stirling, G. H. Lander, J. Rebizant, J. C. Spirlet, D. Gibbs, and O. Vogt, Europhys. Lett. **25**, 137 (1994).
[4] K. Hirota, G. Shirane, P. M. Gehring, and C. F. Majkrzak, Phys. Rev. B **49**, 11 967 (1994).
[5] T. R. Thurston, G. Helgesen, J. P. Hill, D. Gibbs, B. D. Gaulin, and P. J. Simpson, Phys. Rev. B **49**, 15 730 (1994).
[6] A. Tucciarone, H. Y. Lau, L. M. Corliss, A. Delapalme, and J. M. Hastings, Phys. Rev. B **4**, 3206 (1971).
[7] S. R. Andrews, J. Phys. C **19**, 3721 (1986).
[8] T. W. Ryan, R. J. Nelmes, R. A. Cowley, and A. Gibaud, Phys. Rev. Lett. **56**, 2704 (1986).
[9] D. F. McMorrow, N. Hamaya, S. Shimomura, Y. Fujii, S. Kishimoto, and H. Iwasaki, Solid State Commun. **76**, 443 (1990).
[10] G. Shirane, R. A. Cowley, M. Matsuda, and S. M. Shapiro, Phys. Rev. B **48**, 15 595 (1993).
[11] M. E. Fisher and R. J. Burford, Phys. Rev. **156**, 583 (1967).
[12] F. Harbus and H. E. Stanley, Phys. Rev. Lett. **29**, 58 (1972).
[13] F. Harbus and H. E. Stanley, Phys. Rev. B **8**, 1141 (1973).
[14] A. J. Guttmann, J. Phys. C **5**, 2460 (1972).
[15] Y. M. Seidov and G. R. Shaulov, J. Phys. Condens. Matter **6**, 9621 (1994).
[16] N. Bernhoeft, A. Stunault, C. Vettier, F. de Bergevin, Doon Gibbs, T. R. Thurston, S. M. Shapiro, J. B. Hastings, P. Dalmas, G. Helgesen, and O. Vogt, J. Magn. Magn. Mater. **140–144**, 1421 (1995).
[17] P. Erdos and J. M. Robinson, *The Physics of Actinide Compounds* (Plenum, New York, 1983), Chap. 2.
[18] J. Schoenes, B. Frick, and O. Vogt, Phys. Rev. B **30**, 6578 (1984).
[19] M. Kamimoto, Y. Takahashi, and T. Mukaibo, J. Phys. Chem. Solids **37**, 719 (1976).
[20] S. Takagi, N. Nhtsuma, T. Yoshida, and T. Kasuya, J. Phys. Soc. Jpn. **56**, 2287 (1987).
[21] S. L. Carr, C. Long, W. G. Moulton, and M. Kuznietz, Phys. Rev. Lett. **23**, 786 (1969).
[22] H. Rudigier, H. R. Ott, and O. Vogt, Phys. Rev. B **32**, 4584 (1985).
[23] R. Troć and D. J. Lam, Phys. Status Solidi B **65**, 317 (1974).
[24] O. Vogt, P. Wachter, and H. Bartholin, Physica **102B**, 226 (1980).
[25] G. Busch, F. Hullinger, and O. Vogt, J. Phys. (Paris) Colloq. **40**, C4-62 (1979).
[26] O. Vogt, Physica **102B**, 206 (1980).
[27] S. Takagi, J. Phys. Soc. Jpn. **63**, 12 (1994).
[28] J. A. C. Marples, J. Phys. Chem. Solids **31**, 2431 (1970).
[29] M. Steinitz and J. Grunzweig-Genosser, J. Phys. (Paris) Colloq. **40**, C4-34 (1979).
[30] P. M. Gehring, K. Hirota, C. F. Majkrzak, and G. Shirane, Phys. Rev. Lett. **71**, 1087 (1993).
[31] D. Gibbs, G. Grübel, D. R. Harshman, E. D. Isaacs, D. B. McWhan, D. Mills, and C. Vettier, Phys. Rev. Lett. **61**, 1241 (1988).
[32] D. Gibbs, G. Grübel, D. R. Harshman, E. D. Isaacs, D. B. McWhan, D. Mills, and C. Vettier, Phys. Rev. B **43**, 5663 (1991).
[33] D. B. McWhan, C. Vettier, E. D. Isaacs, G. E. Ice, D. P. Siddons, J. B. Hastings, C. Peters, and O. Vogt, Phys. Rev. B **46**, 5287 (1992).
[34] J. P. Hannon, G. T. Trammell, M. Blume, and D. Gibbs, Phys. Rev. Lett. **61**, 1245 (1988).
[35] J. Luo, G. Trammell, and J. P. Hannon, Phys. Rev. Lett. **71**, 287 (1993).
[36] P. Carra and B. T. Thole, Rev. Mod. Phys. **66**, 1509 (1994).
[37] N. Bernhoeft, A. Stunault, C. Vettier, and D. Wermeille (unpublished).
[38] S. K. Sinha, G. H. Lander, S. M. Shapiro, and O. Vogt, Phys. Rev. B **23**, 4556 (1981).
[39] P. Burlet, S. Quezel, J. Rossat-Mignod, and R. Horyn, Solid State Commun. **55**, 1057 (1985).
[40] R. Horyn, J. Y. Henry, and J. Rossat-Mignot, J. Cryst. Growth **63**, 407 (1983).
[41] G. H. Lander, S. Langridge, W. G. Stirling, W. J. Nuttall, G. Grübel, C. Sutter, A. Stunault, F. de Bergevin, C. Vettier, and N. Bernhoeft (unpublished).
[42] N. Bernhoeft (unpublished).
[43] D. S. Rodbell, Phys. Rev. **7**, 1 (1961).
[44] C. P. Bean and D. S. Rodell, Phys. Rev. **126**, 104 (1962).
[45] S. S. Sidhu, W. Vogelsang, and K. D. Anderson, J. Phys. Chem. Solids **27**, 1197 (1966).
[46] N. Curry, Proc. Phys. Soc. (London) **89**, 427 (1966).
[47] N. Bernhoeft, G. G. Lonzarich, D. McK. Paul, and P. W. Mitchell, Physica **136B**, 443 (1986).
[48] N. Bernhoeft, G. G. Lonzarich, and D. McK. Paul, Physica B **156–157**, 699 (1989).
[49] G. G. Lonzarich and L. Taillefer, J. Phys. C **18**, 4339 (1985).
[50] K. K. Murata and S. Doniach, Phys. Rev. Lett. **29**, 285 (1972).
[51] R. Lipowsky, Phys. Rev. Lett. **49**, 1575 (1982).
[52] N. Bernhoeft and G. G. Lonzarich, J. Phys. Condens. Matter **7**, 7325 (1995).
[53] Y. Shnidman and D. Mukamel, J. Phys. C **13**, 5197 (1980).
[54] P. Bak and F. B. Rasmussen, Phys. Rev. B **23**, 4538 (1981).
[55] I. K. Robinson, Phys. Rev. B **33**, 3830 (1986).
[56] S. M. Durbin, Acta Crystallogr. A **51**, 258 (1995).